RSC Advances

ROYAL SOCIETY OF CHEMISTRY

www.rsc.org/advances

A novel and facile approach was developed to fabricate the monodispersed P(St-*co*-MAA)/CeO_2 composite microspheres, which exhibited excellent catalytic performance in the oxidize degradation of methyl orange.

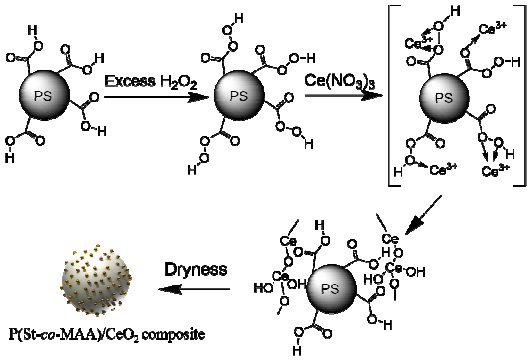

RSC Advances

RSCPublishing

ARTICLE

Preparation of P(St-*co*-MAA)/CeO_2 composite microspheres via surface carboxyl oxidation followed by in situ chemical deposition of CeO_2 and their catalytic application on oxidative degradation of methyl orange

Cite this: DOI: 10.1039/x0xx00000x

Received 00th January 2014,
Accepted 00th January 2014

DOI: 10.1039/x0xx00000x

www.rsc.org/

Guanzhi Cheng, Xinyi Huang, Hong Zhang, Yang Hu, Chengyou Kan*

The modified poly(styrene-co-methyl acrylic acid) (P(St-*co*-MAA)) latex particles were first fabricated via soap-free emulsion polymerization followed by surface carboxyl oxidization, and then the P(St-*co*-MAA)/CeO_2 composite microspheres were prepared through in situ chemical deposition of CeO_2 nanoparticles in the presence of hydrogen peroxide. Then the microspheres were used to catalyze the oxidative degradation of methyl orange (MO) by H_2O_2. The preparation processes were monitored with Fourier transform infrared spectroscopy (FT-IR) and fluorescence spectrophotometry, and the morphology of the composite microspheres was characterized by transmission electron microscopy (TEM) and scanning electron microscopy (SEM). Powder X-ray diffraction (XRD) and nitrogen adsorption–desorption isotherms (BET) were employed to characterize structure and specific surface area of the composite microspheres, respectively. Results showed that the recipe and pH value had significant effects on the morphology of the composite microspheres. When the mass ratio of P(St-*co*-MAA), H_2O_2 and water was 0.1:0.4:9.6, the uniform P(St-*co*-MAA)/CeO_2 composite microspheres were obtained under pH 6.0 using 0.02 mol·L^{-1} of cerous nitrate. The UV-Vis absorption analysis indicated that the apparent rate of MO degradation catalyzed by the composite microspheres was up to 0.0330 min^{-1}, which was 15.7 times as that of the commercial CeO_2. Reusability tests proved that the activity of the composites remained unchanged after underwent 4 cycles. The forming-mechanism of the P(St-*co*-MAA)/CeO_2 composite microspheres was proposed.

Introduction

Since their direct and potential applications in the fields of photonics, medicine, sensors, catalysis and so on, the polymeric/inorganic composite microspheres with tailored physical and chemical properties have been intensively investigated these years.[1-8] Among them, metal or metallic oxide coated polymer composite microspheres, which exhibit core-shell or raspberry-like morphologies, are currently attractive due to their advantages of facile preparation, low density, tunable size and unique surface properties.[9-14] Several approaches have been developed to obtain such composite particles, including sol-gel process, self-assembly process, in situ reduction, and sonochemical deposition.[15-18]

Recently, the composite microspheres with polymer core coated by CeO_2 nanoparticles (NPs) or nanoshells have attracted more attentions because of their advantages on chemical mechanical polishing (CMP). Armini *et al.* fabricated the PMMA/ceria composite microspheres comprising a 300 nm polymer core covered by 14 nm ceria particles through either silane coupling agent modification or electrostatic interactions, and found that these composites could result in less defects after CMP in comparison with conventional slurry material.[19] Chen *et al.* reported an efficient route to fabricate polystyrene/CeO_2 core-shell microspheres with excessive amounts of hexamethylenetetramine as precipitant.[20] Fischer *et al.* prepared PSt/CeO_2 hybrid particles via the functionalization of the PSt core surface with the synthesized surfmers containing phosphonate and phosphate groups.[21] However, because of the high charge density and inert surface of ceria particles, how to simplify the operations, control the composite morphology, improve property and reduce the cost are still challenges for the preparation of polymer/CeO_2 composite microspheres.

CeO_2 has been used as catalyst in oxidative degradation of carbon monoxide, methane and some other organic compounds,[22, 23] but the catalytic properties of the composite microspheres with polymer core anchored CeO_2 NPs have not

been explored. In this study, a novel and facile approach as shown in Fig. 1 was developed for the fabrication of P(St-*co*-MAA)/CeO_2 composite microspheres. Influences of the surface modification and in situ chemical deposition conditions on the morphology of the composite microsphere were investigated, and catalytic performance of the P(St-*co*-MAA)/CeO_2 composite microspheres in the oxidative degradation of MO with H_2O_2 was assayed.

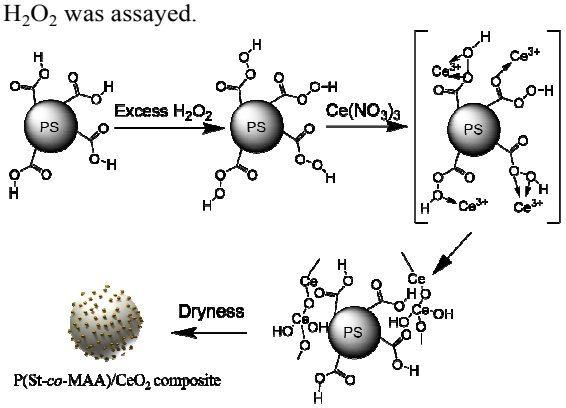

Fig.1 Schematic illustration for the preparation of P(St-*co*-MAA)/CeO_2 composite microspheres.

Experimental

Materials

Styrene (St) and methacrylic acid (MAA) (all A.R. grades, First Chemical Reagent Factory, Tianjin, China) were purified by distillation under reduced pressure. Ammonium persulfate (APS) (A.R. grade, Shanghai Aijian Modern Reagent Co., China) was purified by recrystallization in water before use. $Ce(NO_3)_3$•$6H_2O$, hydrochloric acid (36 wt%), ammonia (25 wt%), cerium dioxide (CeO_2) NPs (99.5%, 20~50 nm), methyl orange (MO) and H_2O_2 (30 wt%) were purchased from Tianjin Guangfu Fine Chemical Research Institute and used as received. Distilled and deionized water was used throughout.

Preparation of P(St-*co*-MAA) seed particles

Monodisperse P(St-*co*-MAA) seed latex was synthesized via soap-free emulsion polymerization,[5] and a typical recipe was given in Table 1. St, MAA and 100 mL of H_2O were first charged into a three-necked 250 ml round-bottom flask equipped with a reflux condenser, a thermometer and a stirrer, and then the flask was immersed in a water bath with constant temperature at 70 ± 0.1 °C. Then, APS dissolved in 25 mL of water was introduced into the flask at the different polymerization time as follows: 12 mL at the beginning, 8 mL at 2 h and 5 mL at 4 h. Subsequently, the system was maintained at 70 °C for an additional 3 h, and cooled down to room temperature to obtain the P(St-*co*-MAA) latex. After that, the latex was purified by centrifuging at 7200 rpm for 15 min and re-dispersing in water three times, and the P(St-*co*-MAA) seed latex with the solid content of 10 wt% was obtained by adjusting the dosage of water.

Table 1 Recipe for the preparation of monodisperse P(St-*co*-MAA) latex

St (g)	MAA (g)	APS (g)	H_2O (mL)
19.33	0.67	0.336	125

Oxidation of surface carboxyl groups of the P(St-*co*-MAA) seed particles

In a typical procedure, 1.0 g of the P(St-*co*-MAA) seed latex, 8.7 ml of water and 0.4 g of H_2O_2 were sequentially added into a test tube and mixed with a Vortex Mixer for 1 min, and the mixture was then kept in dark for 2 h to obtain the oxidized P(St-*co*-MAA) latex.

Preparation of P(St-*co*-MAA)/CeO_2 composite microspheres

P(St-*co*-MAA)/CeO_2 composite microspheres were prepared at 25 °C as follows. At first, pH of the oxidized P(St-*co*-MAA) latex was adjusted to a desired value with hydrochloric acid or ammonia, and 26 mg of $Ce(NO_3)_3$ (0.06 mmol) was dissolved in 3 mL of water in a 10 ml test tube. Then, 500 μL of the oxidized P(St-*co*-MAA) latex was dropwise added into the tube and stirred with the Vortex Mixer for 1 min, and the tube was then standing for a certain time. After that, the mixture was centrifuged at 7200 rpm for 15 min, and the supernatant was saved for the quantitative analysis. The precipitate was washed three times with water by centrifugation, and the composite microspheres were obtained by drying the washed precipitate at 60 °C for 24 h.

As control experiment (A), the P(St-*co*-MAA) latex without oxidation was used to prepare P(St-*co*-MAA)/CeO_2 composite microspheres. As compared to the typical procedure, the difference was that the mixture of P(St-*co*-MAA) latex and H_2O_2 was used immediately to prepare P(St-*co*-MAA)/CeO_2 composite microspheres without kept in dark for 2 h.

As control experiment (B), the surface carboxyl groups of P(St-*co*-MAA) particles were first oxidized with H_2O_2, and the oxidized P(St-*co*-MAA) latex was received by removing the residue H_2O_2 with centrifuging and re-dispersing in water. Then, the oxidized latex was added into $Ce(NO_3)_3$ solution to prepare P(St-*co*-MAA)/CeO_2 composite microspheres.

Catalytic performance assays

To test the catalytic activity of the P(St-*co*-MAA)/CeO_2 composite microspheres, the oxidative degradation of MO was employed as a model reaction. In experiment, 100 ml of 25 mg·L^{-1} MO aqueous solution, 100 mg composite microspheres and 1 ml of H_2O_2 (30 wt%) aqueous solution were sequentially charged into a 250 ml flask with stirring, and the flask was then immersed in a water bath with constant temperature at 75 ± 0.1 °C. pH of the system was kept at 7.0. UV-Vis absorption spectra were recorded at 25 °C in the range of 300-600 nm to monitor the concentration of MO, which exhibits a typical absorption peak at 463 nm at pH 7.0.[24]

The composite microspheres were repeatedly used three times to examine their reusability. After each cycle, the composite microspheres were separated by centrifuging at 7200 rpm for 15 min, and then dispersed in 100 ml 25 mg·L^{-1} fresh MO solution. The following operations were the same as above, and the reaction time was kept at 80 min.

Characterization

Hydrodynamic diameter (D_p^{DLS}), size distribution (poly. index) and zeta potential of the latexes were determined on a dynamic light scattering (DLS) instrument (Zetasizer 3000HS, Malvern, UK) with a fixed scattering angle of 90° at 25 ºC. Morphology and diameter of the dried latex particles (D_p^{TEM}) were characterized using TEM (Hitachi-H7650, Japan) operated at 80 kV. Energy-dispersive X-ray spectroscope (EDS) pattern

and selected area electron diffraction (SAED) pattern were obtained on a high-resolution TEM (HRTEM, JEM-2010, Japan) equipped with EDS and SAED accessories. Scanning electron microscopy (SEM) images were obtained by using a field emission SEM (JEM-7401F, Japan). FT-IR spectra were recorded on a Nicolet 6700 Fourier transform infrared spectrometer operating in the range of 400~4000 cm^{-1}. Excitation and emission spectra were recorded on a fluorescence spectrophotometer (Shimazdu, RF-5301PC, Japan) equipped with a 400 W Xenon lamp as the excitation source. UV-Vis absorption spectra were obtained with a Pgeneral T6 spectrophotometer. Weight loss of the samples was measured on a thermo gravimetric analyzer (TGA, Q5000, TA, USA). Powder X-ray diffraction patterns (XRD) were recorded on a D8 Advance X-ray diffractometer using Cu-Kα radiation (0.1540 nm), and operated at 40 kV × 40 mA. The diffraction patterns were recorded within the range 2θ = 10-90° with a step size of 0.02°. N_2 adsorption-desorption isotherms of the samples were performed on a Micromeritics TriStar II gas adsorption analyzer at 77 K. Samples were dried in an air oven overnight and degassed at 85 °C for at least 60 min, prior to the adsorption measurements.

Results and discussion

Fabrication of P(St-*co*-MAA)/CeO_2 composite microspheres

Properties of P(St-*co*-MAA) seed particles. Soap-free emulsion polymerization is a simple and effective method for preparing monodisperse latex particles.[25] In order to prepare monodisperse particles with surface carboxyl groups, batch soap-free emulsion copolymerization of St and MAA was carried out, and results were given in Table 2 and Fig. 2. It can be seen that the P(St-*co*-MAA) latex particles with the diameter of 360 nm were perfect spheres with a narrow size distribution.

Table 2 Properties of the soap-free P(St-*co*-MAA) latex particles

Conv. (wt %)	D_p^{TEM} (nm)	D_p^{DLS} (nm)	Poly.Index	ζ (mV)
95.6	360	400	0.005	-40.3

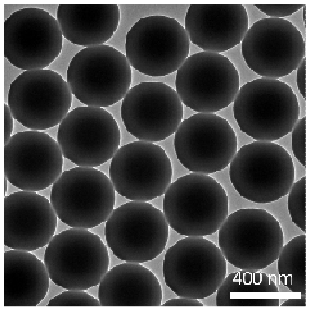

Fig. 2 TEM image of the P(St-*co*-MAA) seed latex.

Oxidation of surface carboxyl of the P(St-*co*-MAA) seed particles. FTIR spectra of the P(St-*co*-MAA) seed particles before and after surface carboxyl oxidation were given in Fig. 3. As compared with the spectrum of the P(St-*co*-MAA) particles, a distinct peak at 1720 cm^{-1} was observed in the spectrum of the oxidized P(St-*co*-MAA) particles, which corresponds to the C=O stretching vibration of peroxycarboxyl groups[26], indicating that carboxyl groups on the P(St-*co*-MAA) particle surface were oxidized to peroxycarboxyl groups.

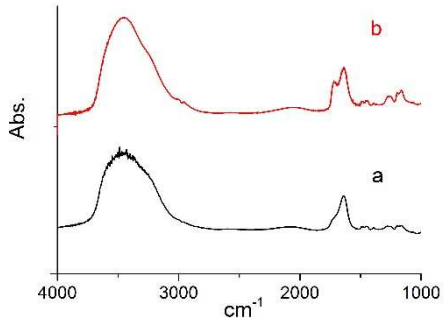

Fig. 3 FTIR spectra of the P(St-*co*-MAA) seed particles before (a) and after (b) surface carboxyl oxidation.

Optimization of deposition time. In order to investigate the relationship between the reaction time and the oxidation extent of Ce^{3+}, fluorescence spectrophotometer was used to test the residual Ce^{3+} in aqueous phase.[27] In experiment, 312 nm and 349 nm were selected as the excitation wavelength and emission wavelength, respectively. The working curve of standard $Ce(NO_3)_3$ solution was drawn at pH 6.0, and the linear regression equation was given in Eq. (1). Coefficient of correlation was 0.9995.

$$F=8.71\times10^5C + 0.001 \quad (1)$$

where F and C represent fluorescence intensity and Ce^{3+} concentration ($mol\cdot L^{-1}$), respectively. The range of linearity was $0\sim10^{-5}$ $mol\cdot L^{-1}$.

Fig. 4 was the reaction time-fluorescence intensity (F) curve of the unreacted Ce^{3+}, and the concentration of residual Ce^{3+} could be calculated by the equation (1). It is clear that the oxidization of Ce^{3+} was very fast, and when the reaction time reached 80 min, the residual Ce^{3+} was only 1 $mmol\cdot L^{-1}$, indicating that over 94% of Ce^{3+} had been oxidized. So, the reaction time was controlled at 2 h subsequently.

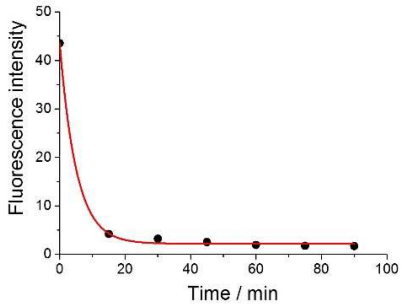

Fig. 4 Reaction time-fluorescence intensity (F) curve of the unreacted Ce^{3+} with 10^4 times dilution.

Influence of the seed latex. It has been demonstrated that both carboxyl and peroxy groups had strong coordination ability to cerium ions[28, 29], and Ce^{3+} could be oxidized by peroxy acid or H_2O_2 to form ceria[30]. Here, the peroxycarboxyl groups on the surface of polymer particles could act as both coordinate groups and oxidation loci of Ce^{3+}, which provided nucleation and structure directing centers for controlled CeO_2 crystallization from solution. So, the P(St-*co*-MAA)/CeO_2 composite microspheres could be fabricated by in situ chemical deposition of CeO_2 NPs on the P(St-*co*-MAA) particle surface under suitable conditions. As Fig. 5 indicated, both the surface carboxyl oxidation of the P(St-*co*-MAA) particles and the residual H_2O_2 were necessary for the formation of P(St-*co*-MAA)/CeO_2 composite microspheres.

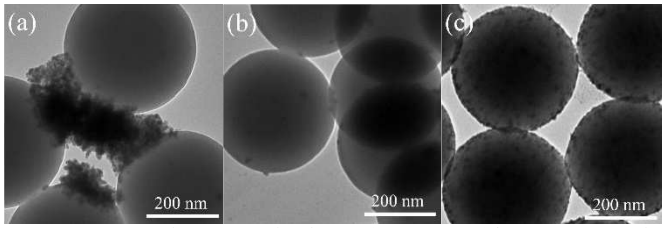

Fig. 5 TEM images of the P(St-*co*-MAA)/CeO_2 composite microspheres prepared using different P(St-*co*-MAA) seed latexes: (a) without surface carboxyl oxidation; (b) with surface carboxyl oxidation and without residual H_2O_2; (c) with surface carboxyl oxidation and residual H_2O_2.

When the un-oxidized P(St-*co*-MAA) particles were used as in control experiment (A), many very small CeO_2 NPs gathered together instead of coated on the surface of the P(St-*co*-MAA) particles (Fig. 5 (a)). Compared to the typical procedure, the difference was that the mixture of P(St-*co*-MAA) latex and H_2O_2 was used immediately to prepare P(St-*co*-MAA)/CeO_2 composite microspheres without kept in dark for 2 h. It is believed that the carboxyl groups on the particle surface could not provide enough coordination ability to cerium ions in comparison with H_2O_2, resulting in the accumulation lacking of cerium ions at the particle surface. On the other hand, since the oxidation process of Ce^{3+} in aqueous phase was very fast, a lot of CeO_2 crystal nucleuses formed and grew in aqueous phase and as a result, few CeO_2 particles were deposited onto the P(St-*co*-MAA) particle surface.

In control experiment (B), the surface peroxycarboxyl groups of the oxidized P(St-*co*-MAA) seed particles could first coordinate with cerium ions and then oxidize Ce^{3+} to form Ce (IV), meaning that some CeO_2 crystal nucleuses would be generated on the particle surface. However, since amount of peroxycarboxyl groups on the particle surface was limited, most of the Ce^{3+} could not be oxidized to Ce (IV) in the absence of H_2O_2. As Fig. 5 (b) demonstrated, only a few CeO_2 NPs were deposited on the particle surface.

When appropriate amount of H_2O_2 was used in the oxidation of surface carboxyl groups, the composite microspheres with CeO_2 NPs on the surface could be obtained as shown in Fig. 5 (c). In this process, when the oxidized P(St-*co*-MAA) latex containing certain amount of H_2O_2 was added into $Ce(NO_3)_3$ solution, the oxygen atoms of peroxycarboxyl groups first coordinated with Ce^{3+}, and then oxidized Ce^{3+} to Ce (IV), which was in situ deposited on the particle surface, forming the primary CeO_2 crystal nucleuses. Subsequently, as the oxidation process continued, the CeO_2 crystals kept growing on the particle surface, and finally the P(St-*co*-MAA) particle surface was covered by CeO_2 NPs.

Influence of H_2O_2 dosage. H_2O_2 dosage must be well controlled, because excess H_2O_2 may cause the direct nucleation of CeO_2 in aqueous phase, while scarce H_2O_2 could not provide enough oxidizing ability to support the continuous crystal growth of CeO_2. Influence of the H_2O_2/H_2O mass ratio on the morphology of P(St-*co*-MAA)/CeO_2 composite microspheres was investigated under pH 7.0, and results were shown in Table 3 and Fig. 6.

The morphology of the composite microspheres was strongly affected by H_2O_2 dosage. With the increase of H_2O_2/H_2O mass ratio, the coverage of the P(St-*co*-MAA) particles with CeO_2 first increased and then decreased, and the optimum mass ratio of H_2O_2/H_2O was 0.4 : 9.6 (Fig. 6 (c)). At a relatively low H_2O_2 concentration, only small amount of Ce^{3+} could be oxidized to Ce (IV), so just a few CeO_2 NPs were observed from the particle surface (Fig. 6 (a)). However, as the carboxyl oxidation is an equilibrium process[31] and the amount of surface carboxyl groups is limited, more H_2O_2 dosage could not form more peroxycarboxyl groups in proportion. In addition, the oxidation rate of Ce^{3+} in aqueous phase increased with the increasing H_2O_2 dosage, and a lot of CeO_2 crystal nucleuses generated and grew up in the aqueous phase. It is clear that at a high H_2O_2 concentration, the oxidation occurred in aqueous phase was dominant, and most of CeO_2 NPs were not coated on the particles as shown in Fig. 6 (e).

Table 3 Influence of H_2O_2 dosage on the morphology of P(St-*co*-MAA)/CeO_2 composite microspheres

Sample	a	b	c	d	e
P(St-*co*-MAA) (g)	0.1	0.1	0.1	0.1	0.1
H_2O_2 (30 wt%) (g)	0.05	0.20	0.40	0.60	0.80
H_2O (g)	9.95	9.80	9.60	9.40	9.20
Diameter of nanoparticles (nm)	1~2	3~4	6~9	/	/

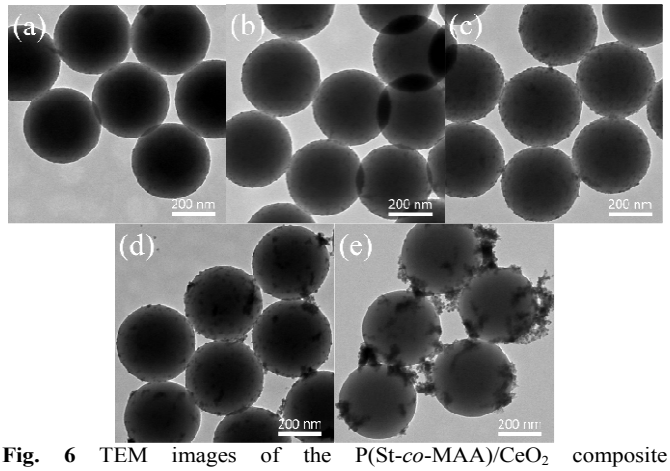

Fig. 6 TEM images of the P(St-*co*-MAA)/CeO_2 composite microspheres prepared with different H_2O_2(30 wt%)/H_2O mass ratio: (a) 0.05 : 9.95; (b) 0.20 : 9.80; (c) 0.40 : 9.60; (d) 0.60 : 9.40; (e) 0.80 : 9.20.

Influence of pH. The morphology of the P(St-*co*-MAA)/CeO_2 composite microspheres was also influenced by the pH of the oxidized P(St-*co*-MAA) latex, and results were given in Fig. 7.

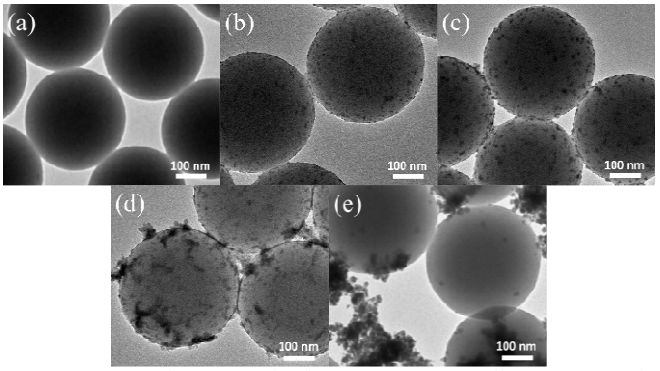

Fig. 7 TEM images of the P(St-*co*-MAA)/CeO_2 composite microspheres prepared at different pH: (a) 2.0; (b) 4.0; (c) 6.0; (d) 8.0; (e) 10.0.

At pH 2.0, since the potential of the Ce^{3+}/Ce^{4+} redox couple was too high based on the Nernst equation[32], it was difficult to oxidize Ce^{3+} to CeO_2. With the increase of pH, the oxidation of

Ce^{3+} became easier as the reduced oxidation potential, and when the pH reached 4.0, CeO_2 NPs were uniformly distributed and strongly anchored on the particle surface. When the pH increased from 4.0 to 6.0, with the increasing coverage, the diameters of CeO_2 NPs anchored on the P(St-*co*-MAA) particle surface increased from 2~3 nm to 7~9 nm as shown in Fig. 7 (b) and Fig. 7 (c). However, under a strong alkaline condition such as pH 10, the oxidation of Ce^{3+} in aqueous phase became dominant and as a result, most of CeO_2 NPs were appeared in aqueous phase (Fig. 7 (e)).

Influence of Ce^{3+} concentration. It has been demonstrated that the Ce^{3+}concentration has an influence on the redox potential and the process of crystal growth.[33] Influence of the $Ce(NO_3)_3$ concentration on the coverage of the P(St-*co*-MAA) particles with CeO_2 was investigated at pH 6.0, and TEM images were given in Fig. 8.

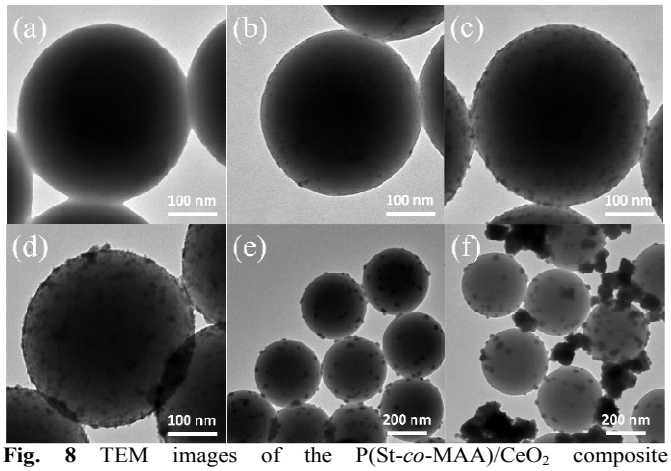

Fig. 8 TEM images of the P(St-*co*-MAA)/CeO_2 composite microspheres prepared with different $Ce(NO_3)_3$ concentration (mmol·L^{-1}): (a) 0.1; (b) 1.0; (c) 10.0; (d) 30.0; (e) 50.0; (f) 70.0.

It is obvious that both the coverage of P(St-*co*-MAA) particle and the size of CeO_2 NPs gradually increased with the increasing concentration of $Ce(NO_3)_3$ from 0.1 mmol·L^{-1} to 30.0 mmol·L^{-1}, and the optimum condition with high coverage and uniform composite structure was achieved in 20.0 mol·L^{-1} $Ce(NO_3)_3$ solution (Fig. 7 (c)). However, if the $Ce(NO_3)_3$ concentration was too high, only a small proportion of Ce^{3+} was coordinated on the particle surface, and most of them was oxidized in aqueous phase. The free CeO_2 NPs nucleated in aqueous phase could easily acquire the rest of cerium ions, which disturbed the subsequent growth of CeO_2 NPs on P(St-*co*-MAA) particle surface.[34] So the coverage of P(St-*co*-MAA) particle even had decreased since the concentration reached 50 mmol·L^{-1}. When the $Ce(NO_3)_3$ concentration reached 70.0 mmol·L^{-1}, many CeO_2 NPs agglomerated in the suspension and deteriorated the formation of CeO_2 NPs on the surface of the polymer particles as shown in Fig. 8 (e).

Morphology and composition of the P(St-*co*-MAA)/CeO_2 composite microspheres

As TEM image (Fig. 7 (c)) shown, when the mass ratio of P(St-*co*-MAA), H_2O_2 and water was 0.1:0.4:9.6, the uniform P(St-*co*-MAA)/CeO_2 composite microspheres were obtained under pH 6.0 using 0.02 mol·L^{-1} of cerous nitrate. The surface morphology and composition of these microspheres were further characterized. SEM image in Fig. 9 (a) showed that the CeO_2 NPs uniformly anchored on the particle surface, and EDS pattern in Fig. 9 (b) also proved the existence of ceria. The size of the CeO_2 NPs in the P(St-*co*-MAA)/CeO_2 composite microspheres in the SEM image was consistent with TEM observation.

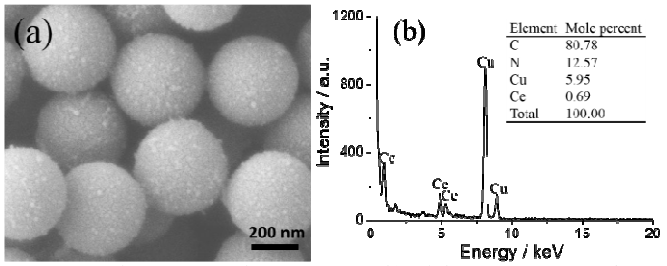

Fig. 9 SEM image (a) and EDS pattern (b) of the P(St-*co*-MAA)/CeO_2 composite microspheres.

The XRD patterns of P(St-*co*-MAA)/CeO_2 composite microspheres and the commercial CeO_2 NPs were given in Fig. 10. The diffraction peaks of commercial CeO_2 NPs were perfectly indexed to the face-centered cubic phase of CeO_2 (JCPDS 34-0394)[35-37]. While the ceria in the P(St-*co*-MAA)/CeO_2 composite microspheres presented as amorphous phase, which is in accord with the cerium oxide precipitates prepared in similar method.[38, 39]

HRTEM image and SAED pattern of P(St-*co*-MAA)/CeO_2 composite microspheres were shown in Fig. 11, indicating that the CeO_2 NPs anchored on the P(St-*co*-MAA) particle surface were amorphous. This result was consistent with what XRD patterns presented.

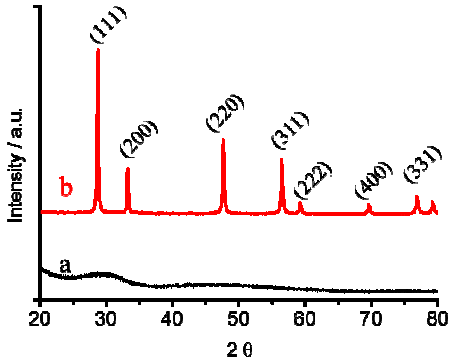

Fig. 10 Powder X-ray diffraction patterns of P(St-*co*-MAA)/CeO_2 composite microspheres (a) and the commercial CeO_2 NPs (b).

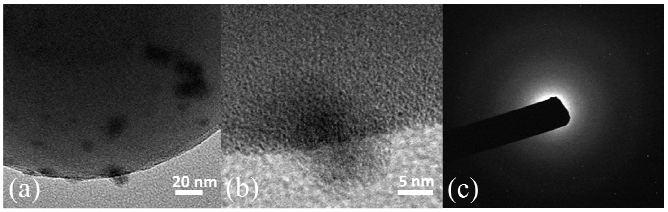

Fig. 11 (a) TEM image, (b) HRTEM image, and (c) SAED pattern of P(St-*co*-MAA)/CeO_2 composite microspheres.

Accurate content of the CeO_2 in the composite microspheres as shown in Fig.9 was analyzed by TGA (Fig. 12). For the pure P(St-*co*-MAA) particle sample, there was almost no weight loss at the temperature below 320 ºC, indicating no change of composition. After that, the weight sharply decreased with increasing temperature, nearly all of the sample was burnt out

above 430 ºC. However, for the composite microspheres, there was a slightly weight decrease from 160℃ to 320 ºC, due to the dehydration of the CeO_{2-x}.[40] At 430 ºC, 8.91% weight was left, and then the weight became constant, indicating the CeO_2 content in the composite microspheres was 8.91 wt%.

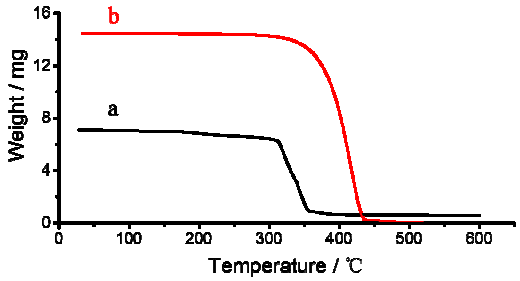

Fig. 12 TGA pattern of the samples: (a) P(St-*co*-MAA)/CeO_2 composite microspheres; (b) pure P(St-*co*-MAA) particles.

The N_2 adsorption desorption isotherms of the samples were presented in Fig. 13. The specific surface area of CeO_2 NPs is calculated to be 9.81 $m^2 \cdot g^{-1}$, while that of P(St-*co*-MAA)/CeO_2 composite microspheres is 16.98 $m^2 \cdot g^{-1}$, suggesting that these composite microspheres possess a higher specific surface area. Considering the CeO_2 content in the composite microspheres was only 8.91 wt%, the real specific surface area of CeO_2 NPs on the surface should be much larger.

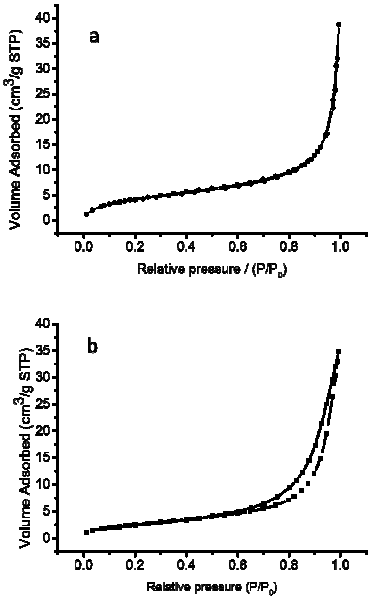

Fig. 13 N_2 adsorption–desorption isotherms of the P(St-*co*-MAA)/CeO_2 composite microspheres (a) and the commercial CeO_2 NPs (b).

Catalytic performance of the P(St-*co*-MAA)/CeO_2 composite microspheres

The P(St-*co*-MAA)/CeO_2 composite microspheres as shown in Fig.9 were employed to evaluate the catalytic performance in the oxidative degradation of MO by H_2O_2. The concentration of MO in the reaction system was measured and used to monitor the reaction progress by recording the absorbance.

Catalytic activity. In the oxidative degradation of MO, the absorption peak of MO at 463 nm gradually dropped its intensity as the reaction proceeded. In experiment, because the concentration of H_2O_2 was much higher than that of MO, it was considered as a constant during the process, and the pseudo-first-order kinetics with respect to MO can be expressed as follows:

$$\ln\left(\frac{C_0}{C}\right) = k_{app}t \quad (2)$$

where k_{app} denotes the apparent oxidative degradation rate constant; C_0 and C express the concentration of MO in the reaction system at the beginning and the reaction time of t, respectively.

In order to assay the catalytic activity of the P(St-*co*-MAA)/CeO_2 composite microspheres, a blank test was carried out by mixing the solution of MO and H_2O_2 in the absence of the composite microspheres. As a control experiment, commercial CeO_2 NPs was directly used as catalyst to replace the composite microspheres, in which the mass of CeO_2 NPs was the same as that of CeO_2 in the composite microspheres based on the TGA results. The dependency of UV-Vis absorption intensity at 463 nm with reaction time for the different reaction systems were shown in Fig. 14. It can be observed that the composite microspheres possessed the highest catalytic activity, and the reaction was almost completed within 80 min (Fig. 14 (a)). In comparison with the blank test, the commercial CeO_2 NPs just showed a slight promotion to the reaction.

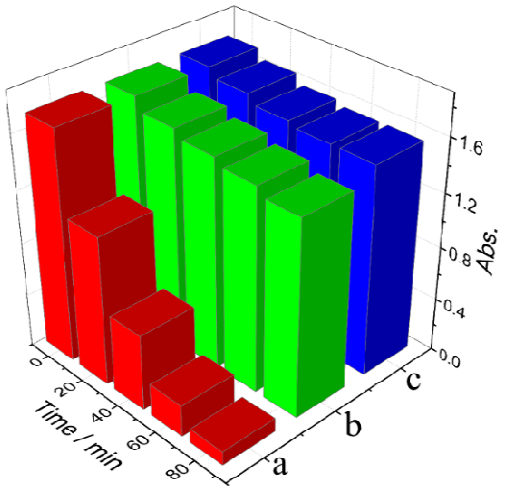

Fig. 14 Variation of UV-Vis absorption intensity versus reaction time for the oxidative degradation of MO catalyzed: (a) with the composite microspheres; (b) with commercial CeO_2 NPs; (c) without catalyst.

The relationship between ln(C_0/C) and reaction time for the MO degradation was drawn in Fig.15, and based on this plot, apparent rate constant (k_{app}) of the oxidative degradation of MO could be calculated. For the reaction systems catalyzed by the composite microspheres (Fig.15 (a)), by the commercial CeO_2 NPs (Fig.15 (b)) and without catalyst (Fig.15 (c)), the value of k_{app} was 0.0330 min^{-1}, 0.0021 min^{-1} and 0.0015 min^{-1}, respectively. The catalytic activity of the composite microspheres was 15.7 times that of the commercial CeO_2 NPs.

The better catalytic performance of the composite microspheres can be attributed to two aspects. The first is its higher specific surface area, because the polymer core can prevent the agglomeration of the CeO_2 NPs. The second is the amorphous structure of CeO_2 NPs, as it has been reported that amorphous CeO_2 exhibits higher catalytic activity than crystalline CeO_2 in the oxidative dehydrogenation of ethylbenzene.[41]

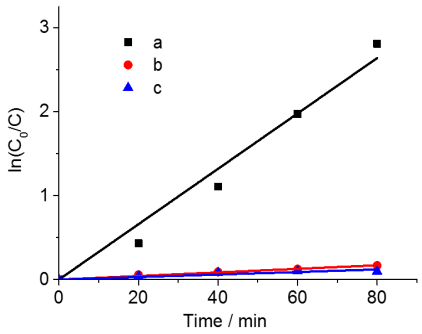

Fig. 15 Kinetics analysis of MO oxidative degradation catalyzed: (a) with the composite microspheres; (b) with commercial CeO_2 NPs; (c) without catalyst.

Reusability. Degradation percentage of MO as a function of the cycle number of the P(St-*co*-MAA)/CeO_2 composite microspheres was examined. Fig. 16 (a) showed that no significant decrease in catalytic activity was observed after reusing three times. TEM image of the four-time used composite microspheres was given in Fig. 16 (b). By comparing the TEM image of the original composite microspheres in Fig. 7 (c), it is clear that the CeO_2 NPs were firmly anchored on the polymer particle surface without pronounced changes after underwent four cycles. This demonstrates that the P(St-*co*-MAA)/CeO_2 composite microspheres had a very good stability and reusability as catalyst.

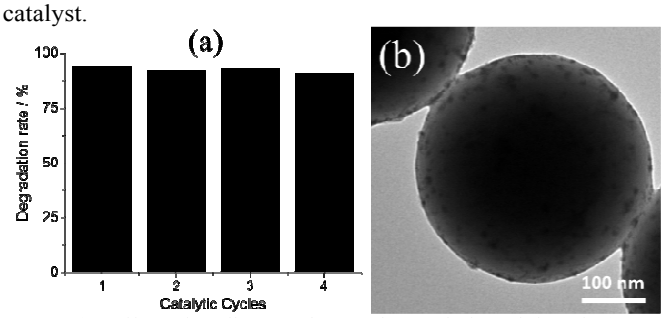

Fig. 16 (a) Effect of cycling number on the catalytic activity of P(St-*co*-MAA)/CeO_2 composite microspheres; (b) TEM image of the P(St-*co*-MAA)/CeO_2 composite microspheres after 4 cycles.

Conclusions

In summary, a novel in situ chemical deposition approach, including sequential the P(St-*co*-MAA) seed preparation, the surface carboxyl oxidation, and the in situ chemical deposition of CeO_2 NPs, was developed for fabricating polymer/CeO_2 composite microspheres. The main factors in the preparation process were systematically investigated to tune the size and coverage of CeO_2 NPs, and when the mass ratio of P(St-*co*-MAA), H_2O_2 and water was 0.1:0.4:9.6, the CeO_2 NPs with diameter of 7~9 nm were firmly anchored on the surface of P(St-*co*-MAA) microspheres under pH 6.0 using 0.02 mol·L^{-1} of cerous nitrate. Furthermore, the obtained P(St-*co*-MAA)/CeO_2 composite microspheres exhibited excellent catalytic activity and reusability, which demonstrates their potential applications in practice.

Acknowledgements

This work is supported by grants from the National Basic Research Program of China (nos. 2014CB932202).

Notes and references

Department of Chemical Engineering and Key Laboratory of Advanced Materials of Ministry of Education of China, Tsinghua University, Beijing 100084, China. E-mail: kancy@tsinghua.edu.cn; Tel: +86 10 6277 3456.

1 T. H. Ji, V. G. Lirtsman, Y. Avny and D. Davidov, *Adv Mater*, 2001, **13**, 1253-1256.
2 L. E. Euliss, S. G. Grancharov, S. O'Brien, T. J. Deming, G. D. Stucky, C. B. Murray and G. A. Held, *Nano Lett*, 2003, **3**, 1489-1493.
3 A. Imhof, *Langmuir*, 2001, **17**, 3579-3585.
4 D. I. Gittins and F. Caruso, *J Phys Chem B*, 2001, **105**, 6846-6852.
5 G. Z. Cheng, W. Deng, Y. Hu and C. Y. Kan, *Acta Polym Sin*, 2012, 111-116.
6 Y. X. Li, Y. Wu, Y. Gao, S. S. Sha, J. F. Hao, G. Q. Cao and C. Yang, *Rsc Adv*, 2013, **3**, 26361-26366.
7 X. M. Feng, *Chinese J Chem*, 2010, **28**, 1359-1362.
8 M. Chen, S. X. Zhou, B. You and L. M. Wu, *Macromolecules*, 2005, **38**, 6411-6417.
9 M. Q. Zhao and R. M. Crooks, *Adv Mater*, 1999, **11**, 217-220.
10 J. Zhou, F. Ren, W. Wu, S. F. Zhang, X. H. Xiao, J. X. Xu and C. Z. Jiang, *J Colloid Interf Sci*, 2012, **387**, 47-55.
11 B. Souder, P. Prashant and S. S. Seo, *Soft Mater*, 2013, **11**, 40-44.
12 W. L. Shi, Y. Sahoo, M. T. Swihart and P. N. Prasad, *Langmuir*, 2005, **21**, 1610-1617.
13 M. Chen, L. Xie, F. Li, S. Zhou and L. Wu, *Acs Appl Mater Inter*, 2010, **2**, 2733-2737.
14 Z. X. Wang, L. M. Wu, M. Chen and S. X. Zhou, *J Am Chem Soc*, 2009, **131**, 11276-11277.
15 C. J. Zhang, X. F. Zhu, H. X. Li, I. Khan, M. Imran, L. Z. Wang, J. J. Bao and X. Cheng, *Nanoscale Res Lett*, 2012, **7**, 1-7.
16 Y. Wu, Y. Zhang, J. Xu, M. Chen and L. Wu, *J Colloid Interface Sci*, 2010, **343**, 18-24.
17 E. Bourgeat-Lami and M. Lansalot, *Adv Polym Sci*, 2010, **233**, 53-123.
18 L. M. Zhao, X. Shao, Y. B. Yin and W. Z. Li, *Mater Res Bull*, 2012, **47**, 2460-2463.
19 S. Armini, J. De Messemaeker, C. M. Whelan, M. Moinpour and K. Maex, *J Electrochem Soc*, 2008, **155**, H653-H660.
20 Y. Chen, J. X. Lu and Z. G. Chen, *Microelectron Eng*, 2011, **88**, 200-205.
21 V. Fischer, I. Lieberwirth, G. Jakob, K. Landfester and R. Muñoz-Espí, *Adv Funct Mater*, 2013, **23**, 451-466.
22 A. Tschope, W. Liu, M. Flytzani-Stephanopoulos and J. Y. Ying, *J Catal*, 1995, **157**, 42-50.
23 S. Scire, S. Minico, C. Crisafulli, C. Satriano and A. Pistone, *Appl Catal B-Environ*, 2003, **40**, 43-49.
24 X. Wang, Y. Liu, Z. Hu, Y. Chen, W. Liu and G. Zhao, *J Hazard Mater*, 2009, **169**, 1061-1067.
25 K. Kang, C. Y. Kan, Y. Du and D. S. Liu, *Eur Polym J*, 2005, **41**, 439-445.
26 E. R. Stephens, P. L. Hanst and R. C. Doerr, *Analytical chemistry*, 1957, **29**, 776-777.
27 D. Ozyurt, B. Demirata and R. Apak, *J Fluoresc*, 2011, **21**, 2069-2076.
28 P. F. Ji, L. Z. Wang, F. Chen and J. L. Zhang, *Chemcatchem*, 2010, **2**, 1552-1554.
29 M. Taguchi, S. Takami, T. Adschiri, T. Nakane, K. Sato and T. Naka, *Crystengcomm*, 2011, **13**, 2841-2848.
30 G. Z. Chen, C. X. Xu, X. Y. Song, S. L. Xu, Y. Ding and S. X. Sun, *Cryst Growth Des*, 2008, **8**, 4449-4453.
31 N. Higashi, H. Yokota, S. Hiraki and Y. Ozaki, *Analytical chemistry*, 2005, **77**, 2272-2277.
32 A. Paulenova, S. E. Creager, J. D. Navratil and Y. Wei, *J Power Sources*, 2002, **109**, 431-438.
33 P. Trinidad, C. P. de Leon and F. C. Walsh, *J Environ Manage*, 2008, **88**, 1417-1425.
34 B. L. Cushing, V. L. Kolesnichenko and C. J. O'Connor, *Chem Rev*, 2004, **104**, 3893-3946.
35 P. Sudarsanam, B. Mallesham, D. N. Durgasri and B. M. Reddy, *Rsc Adv*, 2014, **4**, 11322-11330.
36 K. Kuntaiah, P. Sudarsanam, B. M. Reddy and A. Vinu, *Rsc Adv*, 2013, **3**, 7953-7962.

37 L. Katta, P. Sudarsanam, B. Mallesham and B. M. Reddy, *Catal Sci Technol*, 2012, **2**, 995.
38 B. Y. Johnson, J. Edington and M. J. O'Keefe, *Materials Science and Engineering: A*, 2003, **361**, 225-231.
39 A. M. Shahin, F. Grandjean, G. J. Long and T. P. Schuman, *Chem Mater*, 2005, **17**, 315-321.
40 W. Q. Han, L. J. Wu and Y. M. Zhu, *J Am Chem Soc*, 2005, **127**, 12814-12815.
41 R. Craciun, *Solid State Ionics*, 1998, **110**, 83-93.

